[Faculty Publications](#)   [Chemical Engineering, Department of](#)

1992

Mathematical Modeling of a Primary Zinc/Air Battery

Z. Mao
Texas A & M University - College Station

Ralph E. White
University of South Carolina - Columbia, white@cec.sc.edu

Follow this and additional works at: https://scholarcommons.sc.edu/eche_facpub

Part of the [Chemical Engineering Commons](#)

Mathematical Modeling of a Primary Zinc/Air Battery

Z. Mao* and R. E. White*

Center for Electrochemical Engineering, Department of Chemical Engineering, Texas A&M University, College Station, Texas 77843

ABSTRACT

The mathematical model developed by Sunu and Bennion has been extended to include the separator, precipitation of both solid ZnO and $K_2Zn(OH)_4$, and the air electrode, and has been used to investigate the behavior of a primary Zn-Air battery with respect to battery design features. Predictions obtained from the model indicate that anode material utilization is predominantly limited by depletion of the concentration of hydroxide ions. The effect of electrode thickness on anode material utilization is insignificant, whereas material loading per unit volume has a great effect on anode material utilization; a higher loading lowers both the anode material utilization and delivered capacity. Use of a thick separator will increase the anode material utilization, but may reduce the cell voltage.

Zinc is used widely as an anode in many alkaline batteries, such as Zn/Ni and Zn/Air. Optimum designs of these batteries depend on understanding the zinc chemistry and electrochemistry in alkaline solution and the mass-transport processes in the battery during charge and discharge. While the former has been extensively investigated experimentally, only a few mass-transport models have been presented. Choi, Bennion, and Newman (1) presented a mathematical model of a secondary Zn/AgO battery for analysis of the material redistribution in the battery during charge and discharge. Their model includes convective flow caused primarily by osmosis and electro-osmosis forces. It was found that the convective flow is primarily responsible for the nonuniform zinc distribution on the electrode plate. The validity of their conclusions was verified partially by their experiments that showed virtually no zinc redistribution when the convective flow was minimized (2). Sunu and Bennion (3) developed a comprehensive model of a porous zinc electrode to investigate the electrode phenomena in the direction perpendicular to the projected electrode surface. In their model, the mass-transport equations were developed based on concentrated ternary electrolyte theory. Three electrode failure mechanisms (namely, depletion of hydroxide ions, pore plugging by zinc oxide, and surface passivation) were identified by analyzing the model simulations. The validity of their model was verified by good agreement between their model predictions and experimental data of porosity and zinc oxide distributions (4). Their model was used later by Isaacson et al. (5) and Miller et al. (6) to investigate zinc movement in both the vertical and parallel directions to the electrode surface. Good agreement was obtained by Isaacson et al. (5) between their model predictions and experimental chronopotentiometric data.

It should be noted that all previous mathematical models were used to study secondary batteries and that the model verification was conducted using a half cell or a Zn-NiOOH cell. Previous modeling efforts were focused on the zinc electrode; and, consequently, the concentration distributions in the separator were neglected. Although the findings from such research may be useful for design of a primary Zn-Air battery, many aspects of a primary Zn-Air battery are different from a secondary battery. For example, material redistribution is not of as much concern in a primary battery. Instead, the anode material utilization and polarization behavior are more important. In addition, a primary battery is usually built in the "dry" form, namely, with a gelled electrolyte, and the ratio of the amount of zinc to that of KOH is much greater than that in a secondary battery. The model presented here can be used to analyze the performance of a primary Zn-Air battery with respect to design parameters in order to maximize the performance of the battery.

Chemistry and Electrochemistry

Zinc oxide solubility is relatively high in an alkaline solution because dissolved zinc forms various complexes

* Electrochemical Society Active Member.

with hydroxide ions. These complex ions include $Zn(OH)_4^{2-}$, $Zn(OH)_3^-$, $Zn(OH)_2$, and $Zn(OH)^+$, etc. It is known (7, 8) that only the concentration of $Zn(OH)_4^{2-}$ is appreciable when compared with the other species present in the electrolyte. Therefore, an alkaline zincate solution can be reasonably treated as a ternary electrolyte consisting of KOH, $K_2Zn(OH)_4(l)$, and H_2O. When ionic zinc species (Zn^{2+}) are introduced into the solution by dissolution of Zn, they may remain in the electrolyte as zincate ions or deposit as ZnO (s)

$$Zn(OH)_4^{2-} \rightleftharpoons ZnO(s) + 2\,OH^- + H_2O \qquad [1]$$
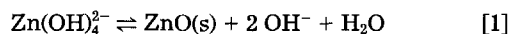
In addition, $Zn(OH)_4^{2-}$ ions can also precipitate in the form of solid $K_2Zn(OH)_4(l)$ if the solution is oversaturated with $K_2Zn(OH)_4$ (9). Although the kinetics of these processes are not clearly understood, a correlation between the alkaline concentration and the solubility of zincate is well established, which is an approximate linear function of hydroxide concentration over a certain range (8).

If zinc remains in the solution as $Zn(OH)_4^{2-}$ and does not precipitate during discharge of a Zn/Air battery, hydroxide ions will be rapidly depleted due to zinc dissolution by OH^- ions, which may cause the cell voltage to increase rapidly. On the other hand, if zincate ions decompose into zinc oxide and hydroxide ions when the solution becomes saturated with zincate, the anodic zinc dissolution would continue as long as the electrode is not blocked by the resulting zinc oxide, and as long as hydroxide ions are available. This availability of OH^- ions depends on the zincate decomposition rate compared to the discharge rate. Unfortunately, it has been reported that the decomposition of zincate ions is a slow process. Also, the precipitation of solid potassium zincate is undesirable because it will result in a loss of potassium hydroxide.

The electrochemistry of zinc anodic dissolution in alkaline solutions has been extensively investigated, as indicated by several review articles on the subject (10-12). However, several reaction mechanisms have been proposed by different researchers, and, unfortunately, agreement about a kinetics expression has not been obtained. It is generally accepted that the anodic zinc dissolution forms zincate ions as follows

$$Zn + 4\,OH^- \rightleftharpoons Zn(OH)_4^{2-} + 2e^- \qquad [2]$$
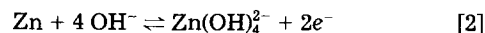
Often the reaction orders of zincate and hydroxide ions obtained from the anodic portion of a polarization curve are different from those obtained from the cathodic portion. The reaction order of hydroxide varies from 1.0 to 3.6, and that of zincate ions changes from 0.65 to 0.9, and the exchange current density varies from 0.5 to 400 mA/cm² (13-16). For engineering purposes, it may be reasonable to use the Butler-Volmer equation as the overall kinetic expression.

If the anodic current density on a zinc electrode is too high, the electrode will become passivated by the coverage of insulating zinc oxide (ZnO). At room temperature, the minimum current density that will cause the passivation is about 100 to 200 mA/cm² (10). For a Zn/Air battery utilizing

a porous zinc electrode, the actual current density is normally lower than this limiting value. Therefore, electrode passivation may be less important than depletion of hydroxide ions and pore plugging by zinc oxide for the Zn/Air battery.

Both solid zinc oxide (ZnO) and solid potassium zincate ($K_2Zn(OH)_4$) are electrical insulators and have higher molar volumes than metallic zinc; consequently, their precipitation in a zinc electrode may cause pore blockage in addition to electrode passivation. Their precipitation rates depend on alkaline concentration, initial electrode porosity, and applied current density.

At the air electrode, oxygen gas undergoes several transport steps before being electrolytically reduced at reaction sites. These steps include transfer into the gas fed porous layer by diffusion and convection in the gas phase, dissolution into the electrolyte, and diffusion in the electrolyte phase to the reaction sites. The overall electrochemical reduction is generally expressed as

$$O_2 + 2H_2O + 4e^- \rightleftharpoons 4\,OH^- \qquad [3]$$
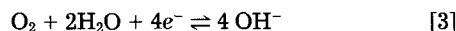
Oxygen solubility and the electrode kinetics dominate the electrochemical behavior of this electrode. The kinetics of an oxygen electrode have been investigated extensively due to its applications in fuel cells and other important electrochemical industries. The kinetics of this electrode reaction depend on the catalyst used, but are generally very slow compared to that of zinc oxidation at the anode. The oxygen solubility in KOH solution is relatively small, and becomes much smaller in a highly concentrated electrolyte, and consequently, the electrode may suffer a significant voltage loss due to concentration polarization.

Development of the Mathematical Model

Since the validity of the mathematical model for a porous zinc electrode by Sunu and Bennion (3) has been verified by their experiments (4) and by others (5), this work consists of extending their model to include the features of a primary Zn/Air battery and including the separator region and the air electrode. The model consists of mass conservation equations, Ohm's law in the solution phase and in the solid phase of the zinc electrodes, a volume balance for the solid phase, and kinetic rate expressions for zinc dissolution, oxygen reduction, and zinc oxide and potassium zincate formation. Diffusion and migration are included in the mass-transport equations. The macro homogeneous approach (17, 18) is used to develop the model.

Porous zinc electrode.—A general mass balance for species i in the electrolyte phase can be written for one dimension as (17)

$$\frac{\partial \epsilon C_i}{\partial t} = -\frac{\partial N_i}{\partial x} + R_i' \qquad [4]$$

where N_i represents the flux of species i, and R_i' accounts for the concentration change rate due to electrochemical and chemical reactions. Application of Eq. [4] for each ionic species yields

$$\frac{\partial \epsilon C_1}{\partial t} = -\frac{\partial N_1}{\partial x} + \frac{1}{nF}\frac{\partial i_2}{\partial x} + R_1 \qquad [5]$$

$$\frac{\partial \epsilon C_2}{\partial t} = -\frac{\partial N_2}{\partial x} - \frac{4}{nF}\frac{\partial i_2}{\partial x} + R_2 \qquad [6]$$

where subscripts, 1 and 2 represent $Zn(OH)_4^{2-}$ and OH^-, respectively, and R_1 and R_2 account for the contribution due to the precipitation of solid zinc oxide and potassium zincate, as presented later.

Since the electrolyte is immobilized by an added gelling agent in a primary Zn/air battery, the solution convection is probably insignificant and, consequently, is not included here. Also, the effect of the interaction between potassium hydroxide and zincates on the transport process is not included, which probably does not introduce an appre-

ciable error to the model predictions, as indicated by the model simulations presented by Sunu and Bennion (3) and Isaacson *et al.* (5). Therefore, based on the derivations by Sunu and Bennion (3), the fluxes, N_1 and N_2 can be expressed as

$$\frac{N_1}{\nu_{1A}} = -D_A \epsilon^{1+\tau}\frac{\partial C_A}{\partial x} + \frac{t_1}{z_1 \nu_{1A} F}\,i_2 \qquad [7]$$

$$\frac{N_2}{\nu_{2B}} = -D_B \epsilon^{1+\tau}\frac{\partial C_B}{\partial x} + \frac{t_2}{z_2 \nu_{2B} F}\,i_2 \qquad [8]$$

where subscripts 1, 2, A, and B represent $Zn(OH)_4^{2-}$, OH^- ions, potassium zincate ($K_2Zn(OH)_4$), and potassium hydroxide, respectively, z_i is the charge number of species i, i_2 is the current density in the solution phase, and τ is a tortuosity factor. The diffusion coefficients D_i ($i = A$ and B) and the transference numbers t_i ($i = 1, 2$) are defined with respect to the volume average velocity v. The symbol ν_{ij} represents the number of ionic species i per molecule for species j.

The current density in the solution phase, i_2, can be calculated using a modified Ohm's law for the ternary electrolyte solution as given by Sunu and Bennion (3)

$$i_2 = -\kappa \epsilon^{1+\tau}\frac{\partial \phi}{\partial x} - \frac{\kappa \epsilon^{1+\tau}}{nF}\left(\frac{s_1}{\nu_{1A}} + \frac{nt_1}{z_1 \nu_{1A}} - \frac{s_o}{C_o}C_A\right)\frac{\partial \mu_A}{\partial x}$$

$$-\frac{\kappa \epsilon^{1+\tau}}{nF}\left(\frac{s_2}{\nu_{2B}} + \frac{nt_2}{z_2 \nu_{2B}} - \frac{s_o}{C_o}C_B\right)\frac{\partial \mu_B}{\partial x} \qquad [9]$$

where ϕ is the potential in the electrolyte relative to a reference electrode of the same kind as the zinc electrode, s_i is the stoichiometric coefficient of species i in reaction [2], κ is the electrolyte conductivity, and μ_i is the chemical potential of species i, which can be related to the concentrations of ionic species as follows (19)

$$\mu_A = \mu_A^o + RT \ln\left[(2C_1 + C_2)^2 C_1 \gamma_A^3\right] \qquad [10]$$

$$\mu_B = \mu_B^o + RT \ln\left[(2C_1 + C_2)C_2 \gamma_B^2\right] \qquad [11]$$

where γ_A and γ_B are the mean activity coefficients of A and B which are assumed to be independent of the electrolyte concentration in this work.

The porosity of the zinc electrode increases as zinc dissolves and decreases as ZnO and $K_2Zn(OH)_4$ precipitate. The rate of change of the porosity is a function of time which can be expressed in terms of the partial molar volumes of zinc, zinc oxide, and potassium zincate and the precipitation reaction rates

$$\frac{\partial \epsilon}{\partial t} = \frac{1}{2F}\overline{V}_{Zn}\frac{\partial i_2}{\partial x} - \overline{V}_{Zn_0}R_{Zn_0O} - \overline{V}_{A_s}R_k \qquad [12]$$

where $\overline{V}_i$ is the partial molar volume of species i ($i = Zn$, ZnO, and $K_2Zn(OH)_4$) and R_{Zn_0O} and R_k are the precipitation rates of solid ZnO and $K_2Zn(OH)_4$, respectively.

The potential in the solid phase of the electrode changes according to Ohm's law

$$i_a = I - i_2 = -\sigma(1 - \epsilon_1)^{1+\tau}\frac{\partial \phi_a}{\partial x} \qquad [13]$$

where I is the applied current density, ϕ_a is the potential in the solid phase, i_a is the current density in the solid phase, and $\sigma(1 - \epsilon_1)^{1+\tau}$ represents the effective electrode conductivity with ϵ_1 representing the porosity related only to metallic zinc. A charge balance for the currents (i_a and i_2) and the electrochemical reaction (reaction [2]) yields the equation

$$\frac{\partial i_a}{\partial x} = -\frac{\partial i_2}{\partial x} = -j_a \qquad [14]$$

where j_a is the transfer current per unit volume of the electrode due to reaction [2], which can be expressed by a Butler-Volmer equation (15, 16)

$$j_a = a_s i_{a,ref} \left\{ \left(\frac{C_2}{C_{2,ref}} \right)^3 \exp \left[\frac{2\alpha_a F}{RT} (\phi_a - \phi - \phi_{a,ref}) \right] \right.$$

$$\left. - \left(\frac{C_1}{C_{1,ref}} \right) \exp \left[- \frac{2(1 - \alpha_a)F}{RT} (\phi_a - \phi - \phi_{a,ref}) \right] \right\} \quad [15]$$

where a_s is the surface area of metallic zinc per unit volume of the electrode which is assumed here to be proportional to $(1 - \epsilon_1)$

$$a_s = a_o \left[\frac{1 - \epsilon_1}{1 - \epsilon^o} \right]^\gamma \quad [16]$$

where γ is a surface effect factor, a_o and ϵ^o are the initial specific surface area and porosity of the zinc electrode, respectively. Since zinc dissolution is due to the electrochemical reaction, ϵ_1 changes according to the equation

$$\frac{\partial \epsilon_1}{\partial t} = - \frac{\bar{V}_{Zn}}{2F} j_a \quad [17]$$

Separator.—The mass-balance equations and the volume-balance equations for both the solid and the electrolyte phases are of the same form as those for the zinc electrode except that no electrochemical reaction occurs in the separator. Also, Ohm's law in the electrolyte is of the same form in this region as that in the zinc electrode.

Precipitation of solid zinc oxide and potassium zincate.—The formation of solid zinc oxide includes the decomposition of zincate ions and the dissolution of zinc oxide at the same time as given in reaction [1]. When the concentration of zincate ions is increased by anodic dissolution of zinc during discharge, the driving force for zinc oxide precipitation is also increased. This additional driving force may be expressed in the terms of oversaturation (20)

$$\Delta G^* = \xi RT (\ln C_1 - \ln C_{1,e}) \quad [18]$$

where ξ represents a correction coefficient and $C_{1,e}$ is the zincate concentration in equilibrium with solid ZnO. On the other hand, the accumulation of zinc oxide causes a rise in its dissolution rate simply because more zinc oxide is available. Therefore, the precipitation rate of zinc oxide may be expressed as

$$R_{ZnO} = k_f \left\{ C_1 \left(\frac{C_1}{C_{1,e}} \right)^\xi - \frac{1}{K} [a_p + k_o(\epsilon_1 - \epsilon)] C_2^2 \right\} \quad [19]$$

where K is the equilibrium constant for reaction [1], a_p is the initial number of moles of ZnO per unit volume of the anode, k_o is a proportional constant, and $(\epsilon_1 - \epsilon)$ represents the volume of the precipitated ZnO if the amount of $K_2Zn(OH)_4$ precipitate is negligible compared to that of ZnO. Similarly, the precipitation rate of solid potassium zincate may be expressed as

$$R_k = k_{f1} C_1 \exp [\zeta(\ln C_1 - \ln C_{1,e}^*)] = k_{f1} C_1 \left(\frac{C_1}{C_{1,e}^*} \right)^\zeta \quad [20]$$

where $C_{1,e}^*$ is the equilibrium concentration of zincate ions with solid potassium zincate, and the reverse reaction is neglected. No experimental data is available for the relation between $C_{1,e}^*$ and alkaline concentration. It is assumed here that $C_{1,e}^*$ also has a linear relation with the concentration of KOH, as shown in Table I. According to reaction [1] and the direct precipitation of potassium zincate, R_1 and R_2 can be written in terms of R_{ZnO} and R_k

$$R_1 = - (R_{ZnO} + R_k) \quad [21]$$

$$R_2 = 2R_{ZnO} \quad [22]$$

Air electrode.—The mass transport in the gas phase is relatively fast compared to that in the liquid phase and, consequently, the mass transport in the gas phase can be treated as if it were a steady-state case. It can be estimated that the mass-transport resistance in the gas phase is negligible compared to that in the electrolyte phase (21). Additionally, the cathode is relatively thin compared to the anode, and the reaction zone is even thinner. Therefore, the cathode can be considered as a flat-plate electrode with a large specific surface area, and its electrochemical behavior can be expressed by the equation

$$I = - a_c \delta i_{c,ref} \left\{ \left(\frac{C_2}{C_{2,ref}} \right)^p \exp \left[\frac{\beta_a F}{RT} (\phi_c - \phi - \phi_{c,ref}) \right] \right.$$

$$\left. - \left(\frac{C_{O_2}}{C_{O_2,ref}} \frac{I_1 - I}{I_1} \right)^q \exp \left[- \frac{\beta_c F}{RT} (\phi_c - \phi - \phi_{c,ref}) \right] \right\} \quad [23]$$

where I_1 represents the limiting current density due to the diffusion of dissolved oxygen in the electrolyte. IUPAC solubility data (22) show that the oxygen solubility and electrolyte concentration has the following relation

$$C_{O_2} = C_{O_2}^o \exp (-k_e C_t) \quad [24]$$

where k_e is a constant with units of cm^3/mol, $C_{O_2}^o$ is the oxygen solubility in pure water, C_t represents the total concentration of the electrolyte. Therefore, the limiting cathodic current density can be further expressed as

$$I_1 = I_{1,ref} \exp [-k_e(C_t - C_{t,ref})] \quad [25]$$

where $I_{t,ref}$ represents the limiting current density at the reference total concentration, $C_{t,ref}$. Consequently, Eq. [23] can be rewritten as

$$I = - a_c \delta i_{c,ref} \left\{ \left(\frac{c_2}{C_{2,ref}} \right)^p \exp \left[\frac{\beta_a F}{RT} (\phi_c - \phi - \phi_{c,ref}) \right] \right.$$

$$- \left[\exp [- k_e(C_t - C_{t,ref})] - \frac{I}{I_{1,ref}} \right]^q$$

$$\left. \exp \left[- \frac{\beta_c F}{RT} (\phi_c - \phi - \phi_{c,ref}) \right] \right\} \quad [26]$$

Summary of the modeling equations.—Equations [5], [6], [9], [12]-[14], [19], and [26] present a complete set of the equations which describe the concentrations of $Zn(OH)_4^{2-}$ and OH^-, the potentials ϕ_a and ϕ, the porosities ϵ and ϵ_1, and current density i_2 as functions of time and position. With proper boundary conditions and initial conditions, the solution of these equations can be obtained by using a numerical method.

Boundary conditions.—Figure 1 shows a schematic view of the model cell, which consists of three boundaries and two regions. At the current collector, namely, the back side of the zinc electrode ($x = 0$), the current density in the solid phase is equal to the applied discharge current density, the current density in the electrolyte phase equals zero, and the flux of each species is zero. At the Zn electrode/separator interface ($x = x_s$), continuity of the fluxes of all species is specified. The current density in the solid phase becomes zero, and the current density in the electrolyte then equals the applied discharge current density. At the cathode ($x = x_1$), it is assumed that the concentrations of all species within the electrode are uniform, and a mass balance for species i must be used to derive the boundary conditions

$$\delta(\epsilon_c - \epsilon_s^o + \epsilon) \frac{\partial C_i}{\partial t} = N_i|_{x=x_1} - \frac{s_{c,i} I}{n_c F} \quad [27]$$

where ϵ_c and ϵ_s^o are initial porosities of the cathode reaction zone and the separator, respectively. The term $(\epsilon_c -$

Table I. Input parameters

Symbol	Parameter	Reference
	Structure parameters	
a_o	1.0×10^3 cm^2/cm^3	†
a_c	10^4 cm^2/cm^3	†
δ	1.0×10^{-2} cm	†
ϵ^o	0.731	
ϵ_s^o	0.6	
ϵ_c	0.5	
x_s	0.4 cm	
x_l	0.42 cm	
σ	10^5 S/cm	†
	Reaction kinetic parameters	
$i_{a,ref}$	30.0×10^{-3} A/cm^2	†
α_a	0.5	15
$\phi_{a,ref}$	-1.353 V	27
p	1.0	†
q	1.0	†
$i_{c,ref}$	1.5×10^{-10} A/cm^2	†
β_a	1.0	†
β_c	1.0	†
$\phi_{c,ref}$	0.301 V	
$I_{1,ref}$	0.5 A/cm^2	†
k_f	1.95×10^{-5} s^{-1}	†
ξ	1	†
a_p	$KC_1^o \left(\dfrac{C_1^o}{C_{1,e}^o}\right)^\xi \Big/ (C_2^o)^2$	‡
k_o	0.2	†
K	3.0×10^{-3} mol/cm^3	†
k_e	0.175×10^3 cm^3/mol	22
k_{fl}	1.8×10^{-9} s^{-1}	†
ζ	3.0	†
s_1	-1	
s_2	4	
s_o	0	
$s_{c,1}$	0	
$s_{c,2}$	4	
z_1	-2	
z_2	-1	
n	2	
n_c	4	
ν_{1A}	1	
ν_{2B}	1	
	Transport property parameters	
D_A	6.0×10^{-6} cm^2/s	5
D_B	2.19×10^{-5} cm^2/s	5
κ	0.45 S/cm	5
τ	0.5	3
t_1	0.01	28
t_2	0.78	3
$\overline{V}_{ZnO}$	14.5 cm^3/mol	3
$\overline{V}_1$	20.0 cm^3/mol	†
$\overline{V}_{Zn}$	9.16 cm^3/mol	3
$C_{1,ref}$	$= C_1^o = 2.3811 \times 10^{-4}$ mol/cm^3	
$C_{2,ref}$	$= C_2^o = 8.0 \times 10^{-3}$ mol/cm^3	
$C_{1,e}$	$= 1.0 \times 10^{-1} C_2$ mol/cm^3	8
$C_{1,e}^*$	$= 1.0 \times 10^{-1} C_2$ mol/cm^3	†
	Operating parameters	
T	298.15 K	

† Arbitrarily chosen. k_f, k_{fl}, and $i_{a,ref}$ were chosen so that the predicted discharge curve agrees with the experimental data at 20 mA/cm^2 provided by MATSI, Inc. (24).

‡ Chosen so that the initial precipitation rate of ZnO is zero.

$\epsilon_s^o + \epsilon$) represents the porosity of the cathode reaction zone. The symbol $s_{c,i}$ is the stoichiometric coefficient of species i in the cathode reaction (see reaction [3]). The current density in the electrolyte is equal to the applied discharge current density.

Initial conditions.—A certain amount of zinc oxide is usually intentionally added to the electrolyte to prevent the self discharge of the zinc electrode. The initial zincate concentration can be estimated from the known added amount of ZnO. The initial concentration of hydroxide ions is as prepared if the amount of zinc oxide is small compared to the amount of KOH. Before the battery is discharged, it is assumed here that the concentration of each
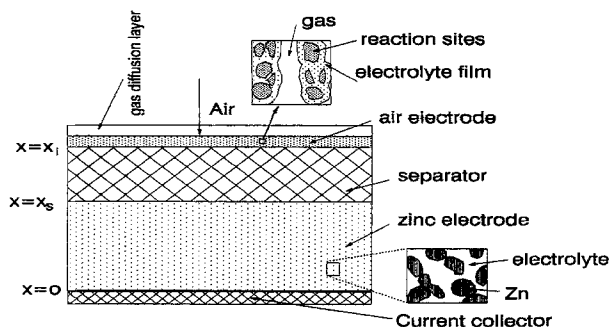

Fig. 1. Schematic view of the model regions.

species is uniformly distributed throughout each part of the battery.

Numerical Solution

A finite-difference method is used to solve the model equations. The differential equations were discretized using the Crank-Nicolson approximation, and the resulting algebraic equations were solved using the iterative Newton-Ralphson method with the algorithm developed by Newman (23).

Although the initial electrode potentials (ϕ_a, ϕ, and ϕ_c) in both the solid phases in the anode and the cathode and in the electrolyte phase are not needed, initial guesses for these three variables are required for the iteration method. It was found that their values are critical for obtaining a converged solution for the first time step. To obtain values close to the solution, the initial guess values were obtained as follows. The electrode potential in the solid phase at the cathode (ϕ_c) was set to a given value ($\phi_{c,ref}$); then the potential in the solution at the cathode was estimated by solving Eq. [26]

$$\phi(x_l) = \phi_c - \phi_{c,ref} + \frac{RT}{\beta_a F} \ln X_c \qquad [28]$$

where

$$X_c = \frac{I + \sqrt{I^2 + 4YZ}}{2Y} \qquad [29]$$

$$Y = a_c \delta j_{c,ref} \left(\frac{C_2^o}{C_{2,ref}}\right)^p \qquad [30]$$

$$Z = a_c \delta j_{c,ref} \left[\exp\left[-k_e \left(C_t^o - C_{t,ref}\right)\right] - \frac{I}{I_{1,ref}}\right]^q \qquad [31]$$

The potential in the separator can be assumed to be linearly distributed, and, consequently, the potential in the solid phase at the anode can be estimated by solving the equation

$$I = x_s a_o j_{a,ref} \left\{ \left(\frac{C_2^o}{C_{2,ref}}\right)^3 \exp\left[\frac{2\alpha_a F}{RT}(\phi_a(x_s) - \phi(x_s) - \phi_{a,ref})\right] \right.$$

$$\left. - \left(\frac{C_1^o}{C_{1,ref}}\right) \exp\left[-\frac{2(1 - \alpha_a)F}{RT}(\phi_a(x_s) - \phi(x_s) - \phi_{a,ref})\right] \right\} \qquad [32]$$

As shown in Fig. 1, the adjustable design parameters are the electrode thickness (x_s), the initial zinc loading (related to ϵ^o), initial zincate concentration (C_1^o), initial KOH concentrations (C_2^o), gelling agent content (upon which the diffusion coefficient of each species and electrolyte conductivity depend), and the separator thickness ($x_l - x_s$). An

exploration for the optimum values of these parameters has been conducted by varying these parameters as described below in the Results and Discussion section. All fixed input parameters for the program are listed in Table I.

Since the solution of the model equations yields the concentrations, porosity, and the potentials as a function of position and time, other dependent variables such as the cell voltage, each component of the cell voltage loss, and the anode material utilization can be calculated as follows. The cell voltage is the potential difference at the current collector ($x = 0$) and at the cathode ($x = x_l$): $E = \phi_c - \phi_a$. Cell voltage loss is due to the overpotential at the anode (η_a), ohmic loss across the separator (η_s), and the overpotential at the cathode (η_c). The anode material utilization for a given cutoff cell voltage can be calculated from the time to the cutoff cell voltage and the applied current density

$$\theta_u = \frac{\dfrac{\overline{V}_{Zn}}{2F} It}{(1 - \epsilon^o)x_s} \times 100\% \qquad [33]$$

or from the electrode porosity change at the cutoff cell voltage

$$\theta_u = \frac{(1 - \epsilon^o)x_s - \int_0^{x_s}(1 - \epsilon_l)dx}{(1 - \epsilon^o)x_s} \times 100\% \qquad [34]$$

Results and Discussion

A comparison of the discharge curves between the model prediction and the experimental data provided by MATSI, Inc. (24) is presented in Fig. 2 for the battery specifications given in Table I. There are some discrepancies between the two sets of experimental data, probably because some uncertain experimental conditions may be involved. Although no attempt was made to fit the model prediction to the experimental data by using a parameter estimation technique, the model prediction curve was adjusted to be close to the experimental data by manually changing three parameters: the exchange current density for the zinc electrode reaction ($i_{a,ref}$), and the two reaction rate constants for the precipitation of solid zinc oxide and solid potassium zincate (k_f and k_{fl}). The exchange current density for the
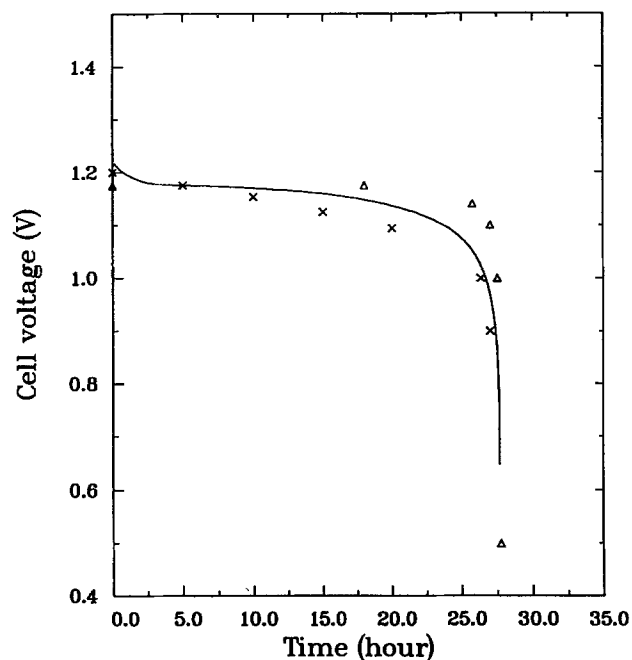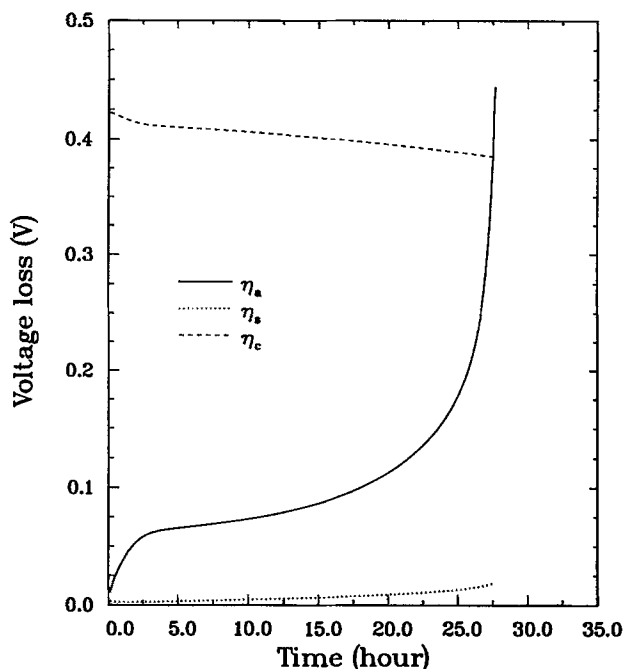
Fig. 3. The predicted potential loss at each part of the cell as a function of time. The input parameters are the same as those for Fig. 2.

zinc electrode reaction was chosen within the range of those reported in the literature, while the other two parameters (k_f and k_{fl}) were chosen arbitrarily. It can be seen from Fig. 2 that there is good agreement between the model predictions and the experimental data. The model predictions indicate that there is a rapid drop in cell voltage during the initial state of discharge, which is the expected behavior of a Zn/Air battery (25, 26). Depletion of hydroxide ions is responsible for this cell voltage drop. Following the initial drop is a plateau which extends almost to the end of discharge. Further interpretation of the discharge behavior is presented next by analyzing each component of the cell voltage loss and the distributions of the potential in the solution, the transfer current per unit volume, and the concentrations.

The cell voltage loss is attributed to the overpotentials at both the anode and cathode and the ohmic drop across the separator. Figure 3 shows the model predictions for each component of the cell voltage loss as a function of time. The overpotential at the anode is defined by the difference between the potential in the solid phase and that in the electrolyte adjacent to the electrode surface at $x = x_s$

$$\eta_a = \phi_a(x_s) - \phi(x_s) - \phi_{a,ref} \qquad [35]$$

The ohmic drop across the separator is defined by the potential difference in the electrolyte at the cathode and at the anode near the separator/the electrode interfaces

$$\eta_s = \phi(x_s) - \phi(x_l) \qquad [36]$$

and the overpotential at the cathode is defined similarly to that at the anode

$$\eta_c = \phi_c - \phi(x_l) - \phi_{c,ref} \qquad [37]$$

Although the cathode is a major source for cell voltage loss because of the slow kinetics for oxygen reduction, the overpotential at the cathode decreases slightly during discharge because the oxygen solubility increases as the electrolyte concentration decreases during discharge. The voltage loss across the separator increases continuously during discharge because both the porosity and the electrolyte concentration decrease, and consequently, the effective electrolyte conductivity is decreased. However, the voltage loss across the separator is negligible compared to those at the anode and the cathode. The overpotential at the anode increases rapidly at the beginning of discharge, reaches a near-plateau region, and finally increases sharply

Fig. 2. Comparison between model prediction and the experimental data provided by MATSI, Inc. $I = 20$ mA/cm^2, the input parameters for the program are listed in Table I. The symbols represent two sets of experimental data obtained under the same conditions, and the solid line is the model prediction.
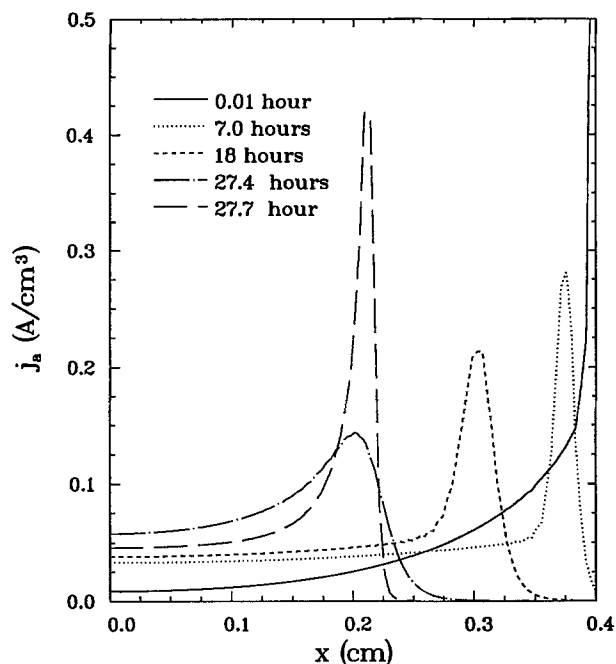
Fig. 4. The predicted transfer current per unit volume as a function of position at different states of discharge. The input parameters are the same as those for Fig. 2.
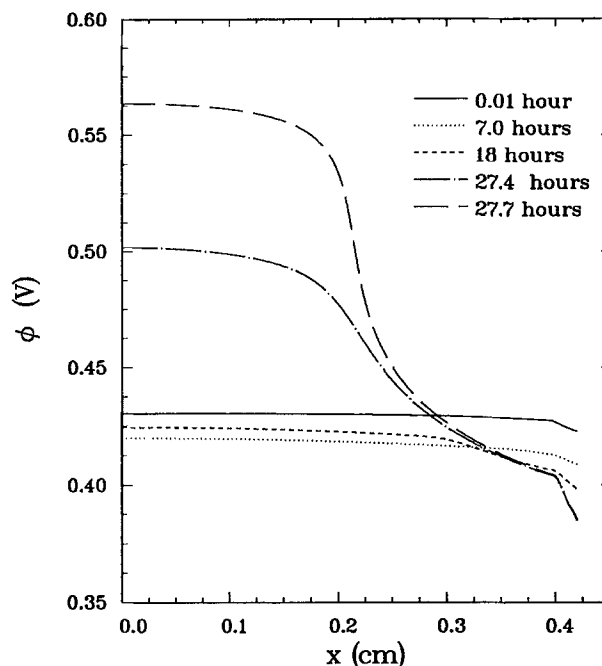

Fig. 5. The potential in the electrolyte phase as a function of position at different states of discharge. The input parameters are the same as those for Fig. 2.

at the end of discharge. Evidently, the zinc electrode behavior determines the battery performance.

Since the kinetics of the zinc electrode reaction are fast, the reaction rate is sensitive to the reactant concentration and the electrode potential. Figure 4 shows the predicted transfer current per unit volume as a function of the position. The anodic reaction preferentially occurs in the front side of the electrode, as if the transfer current were limited within a very narrow region. This reaction zone does not expand significantly, but gradually moves into the electrode. This is because the reactant (OH^-) is more available and because the driving force for the reaction (potential difference) in the front side of the electrode is higher than that at the back side. At the end of discharge, a sharp peak forms in the middle of the electrode due to a sharp shift in the potential in the electrolyte and a rapid change in the OH^- concentration as shown in Fig. 5 and Fig. 8.

Figure 5 shows the predicted potential in the electrolyte as a function of position. The potential shifts gradually in the negative direction, which causes a rise in the driving force for the reaction at the anode as the discharge proceeds. At the end of discharge, the potential shifts significantly in the positive direction in the region toward the back side of the electrode. Since the discharge is carried out at a constant current, the anode reaction is forced to occur at a constant rate; consequently, the electrode potential in the solid phase is drawn to a very positive value to retain the same current. This occurs because the zinc material in the front side of the electrode has been depleted, and hydroxide ions are available from the cathode; therefore, the potential in the electrolyte shifts as shown in Fig. 5.

Figure 6 presents the predicted porosity as a function of position at different states of discharge. The solid phase in the electrode consists of solid metallic zinc, zinc oxide, and potassium zincate. The porosity change is the net result of zinc dissolution and the precipitation of both zinc oxide and solid potassium zincate. As shown in Fig. 6, the zinc in the front side of the electrode is preferentially dissolved at an early state of discharge. The resulting zincate ions diffuse away from this region because the electrolyte is not saturated initially with zincate ions and the precipitation of zinc oxide is a slow process. As a result, the porosity in the front side of the electrode increases at the beginning. However, when zinc oxide and potassium zincate start to precipitate and accumulate in the electrode as the discharge proceeds, the electrode porosity decreases. On the

other hand, the porosity in the separator decreases continuously because the precipitated zinc oxide and potassium zincate accumulate continuously in this region. Therefore, it may be inferred that pore blockage is unlikely to occur in the zinc eletrode; however, it may occur in the separator.

Figures 7 and 8 show the predicted concentration profiles of zincate and hydroxide ions at different states of discharge. The concentration of zincate ions increases rapidly with time at an early state of discharge and decreases at later states of discharge because the precipitation of zinc oxide is a slow process, which results in a buildup in the zincate concentration. On the other hand, the concentration of hydroxide ions decreases continuously, causing a rapid rise in the zincate saturation level, and, consequently, accelerating precipitation of zinc oxide and potas-
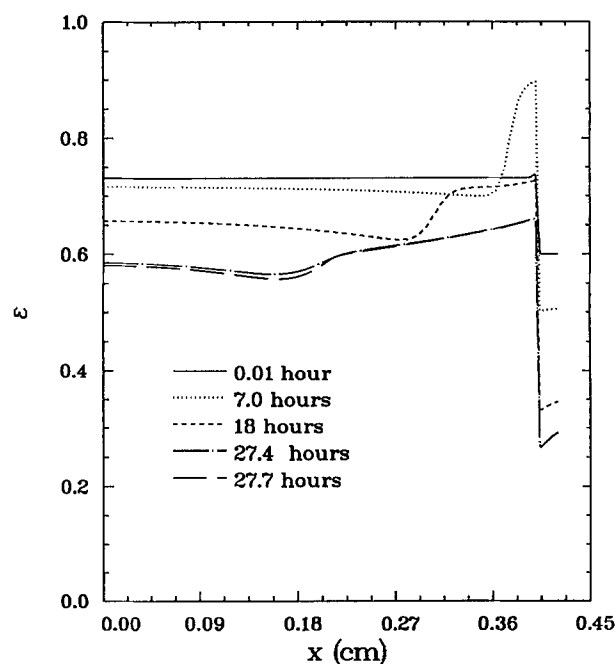

Fig. 6. The predicted porosity as a function of position at different states of discharge. The input parameters are the same as those for Fig. 2.
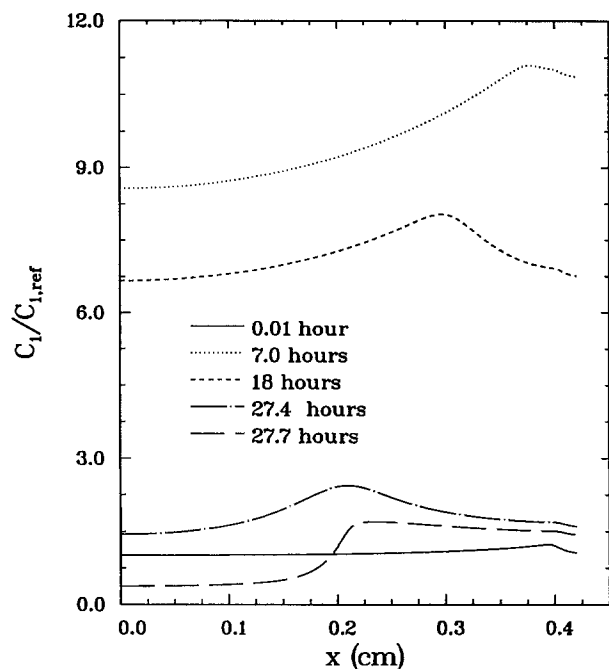
Fig. 7. The predicted concentration profiles for zincate ions at different states of discharge. The input parameters are the same as those for Fig. 2.
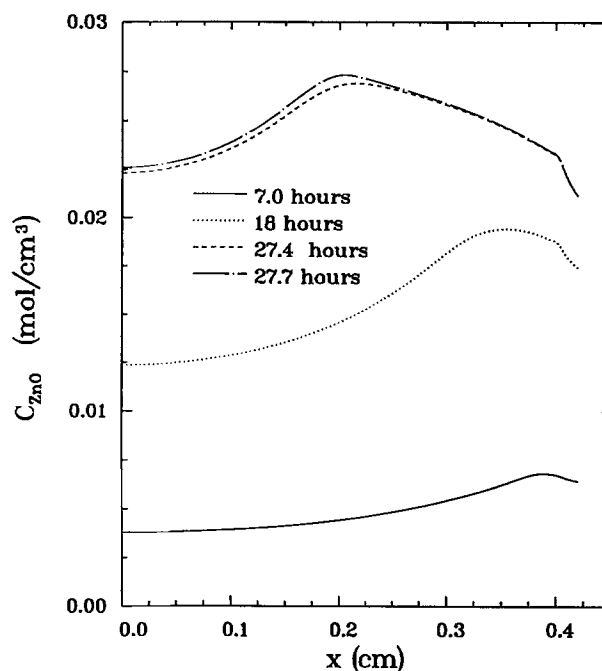

Fig. 9. The solid zinc oxide distributions at different states of discharge. The input parameters are the same as those for Fig. 2.

sium zincate. As described earlier, zinc oxidation occurs within a narrow zone, and this zone moves into the electrode. Correspondingly, the highest zincate concentration appears near the reaction zone, and this concentration peak becomes broader and gradually moves into the electrode as shown in Fig. 7. The concentration of the hydroxide ions decreases with discharge, but is larger near the cathode as expected (Fig. 8).

Figures 9 and 10 show the solid zinc oxide and solid potassium zincate as a function of position at different states of discharge. As expected, the amount of zinc oxide increases with discharge time, and its distribution is similar to that of potassium zincate. As shown in Fig. 10, the amount of solid potassium zincate increases near the end

of discharge. This process will result in a rapid decrease in the concentration of hydroxide ions, and, consequently, will lead to electrode failure. It should be noted that the predicted amount of solid potassium zincate is small compared to that of ZnO.

Figure 11 shows the predicted discharge curves at different discharge rates. The predicted cell voltage increases, and the plateau region becomes flatter as the discharge rate decreases. Furthermore, the anode material utilization decreases with increasing discharge rate as indicated by the cell voltage reading 0.9 V at a lower state of discharge. The predicted discharge curves shown in Fig. 11 are qualitatively consistent with experimental data reported in the literature. However, at the high discharge rate, it appears that the predicted anode material utilization is
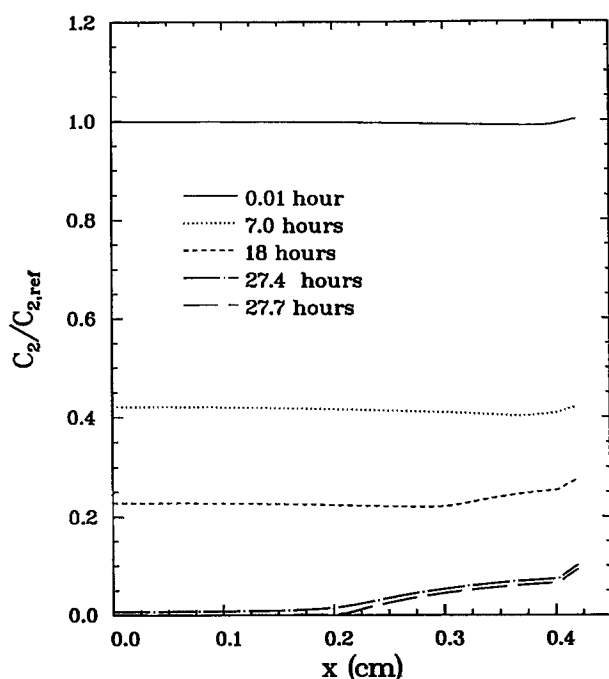

Fig. 8. The predicted concentration profiles for hydroxide ions at different states of discharge. The input parameters are the same as those for Fig. 2.
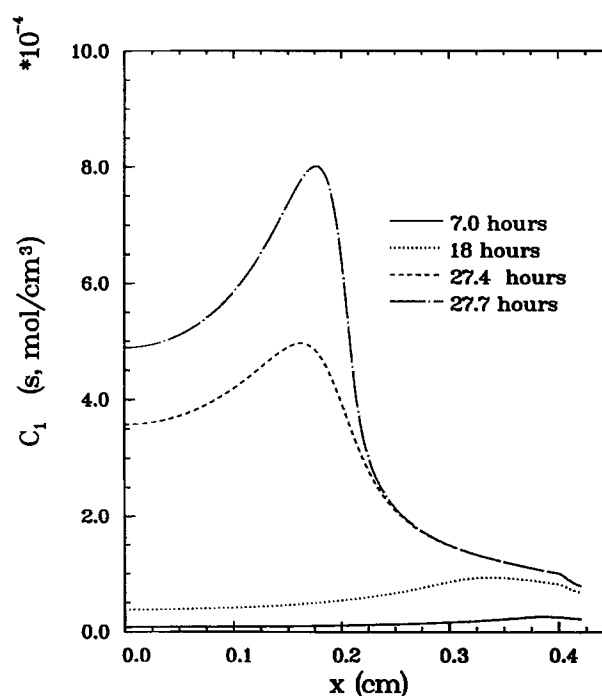

Fig. 10. The solid potassium zincate distributions at different states of discharge. The input parameters are the same as those for Fig. 2.
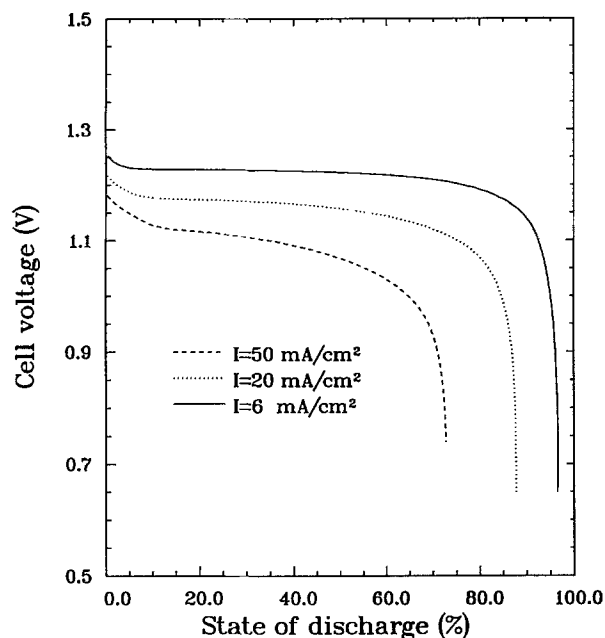
Fig. 11. The predicted cell voltage as a function of state of discharge at different discharge rates. The other input parameters are the same as those for Fig. 2.

Fig. 13. The predicted cell voltage as a function of state of discharge at different electrode thicknesses. The other input parameters are the same as those for Fig. 2.

higher than that normally observed experimentally. One possible explanation for this is that the passivation of the zinc electrode due to zinc oxide precipitation may be an important factor in the electrode failure at a high discharge rate; this factor has not been included in the model.

The material loading is an important parameter in designing a zinc electrode. The optimum material loading is affected by many factors such as the electrolyte concentration, electrode thickness, and discharge rates. Figure 12 shows the predicted cell voltage as a function of state of discharge for electrodes loaded with different amounts of zinc. The electrode with a theoretical capacity of 630 mAh/cm^2 has an initial porosity of 0.731, the capacities of the other two electrodes are increased by 20% and 40% from this base case, respectively, giving the electrode porosities of 0.677 and 0.623. It is generally expected that the material utilization may decrease, but the delivered capacity may

increase or at least be the same as the material loading level is increased. However, Fig. 12 indicates that both the material utilization and the delivered capacity decrease as the material loading is increased. This may be due to less electrolyte being available for a higher material loading.

Figure 13 shows the predicted discharge curves for different electrode thicknesses. By increasing the electrode thickness, the electrode capacity can be increased if the material utilization is the same. Figure 13 indicates that such a means is effective in increasing electrode capacity. Experimental data (24) also show that the material utilization is almost the same for the electrode thicknesses of 0.4 and 0.5 cm at the discharge current density of 20 mA/cm^2. Therefore, the model predictions are consistent qualitatively with the experimental data.
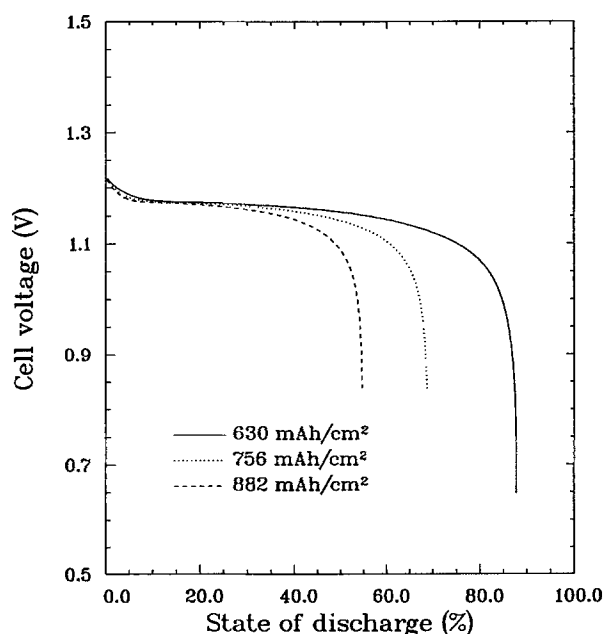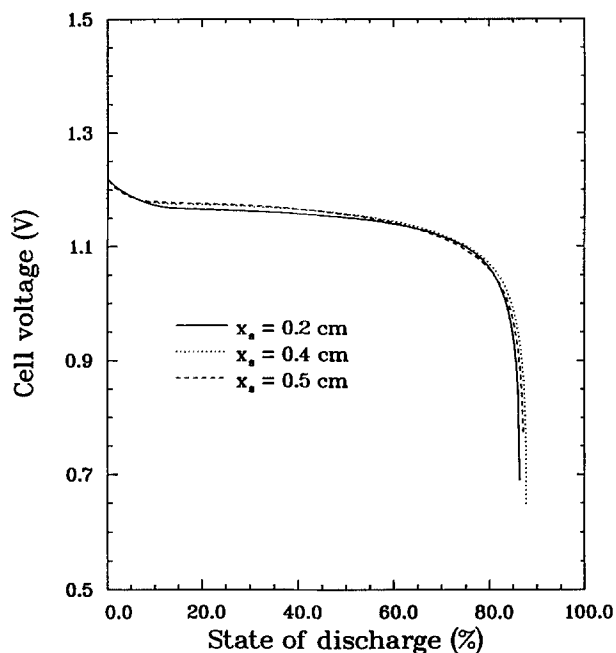

Fig. 12. The predicted cell voltage as a function of state of discharge for electrodes with different zinc loading. The other parameters are the same as those for Fig. 2.
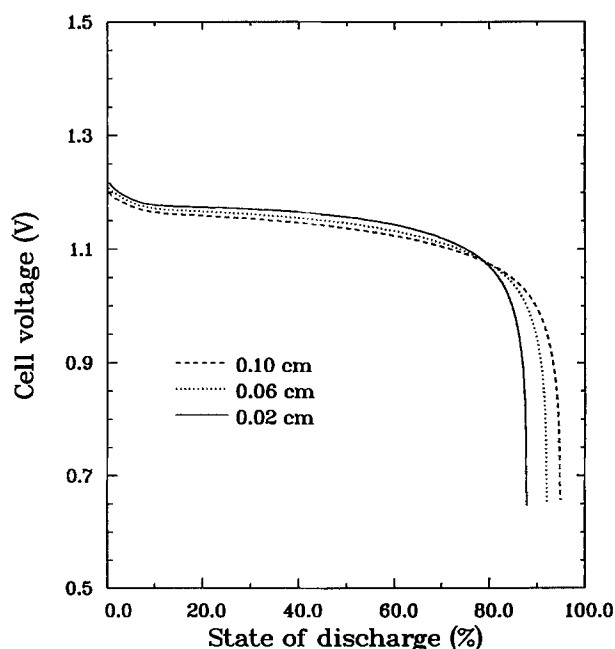

Fig. 14. The predicted cell voltages as a function of discharge state for different separator thicknesses. The other input parameters are the same as those used for Fig. 2.
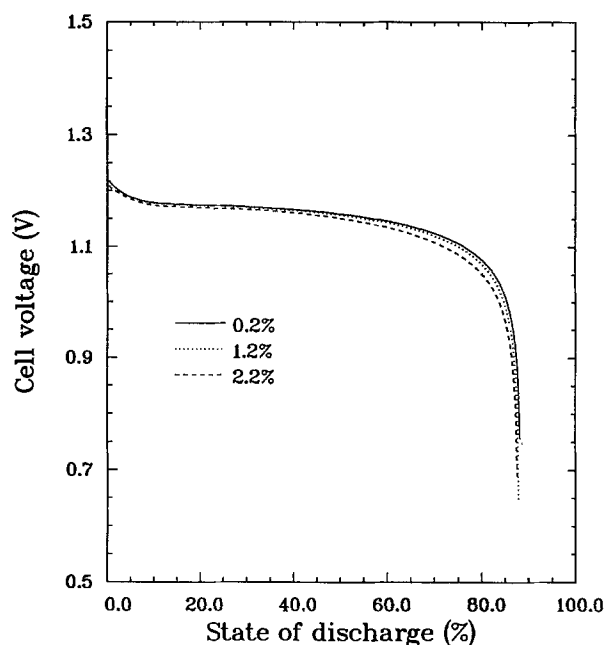
Fig. 15. The predicted cell voltage as a function of state of discharge at different gelling content in the electrolyte. The other input parameters are the same as those for Fig. 2.

It is generally thought that to reduce the internal resistance of a Zn/Air battery the separator thickness should be reduced to a minimum. Figure 14 shows the predicted cell voltage as a function of discharge state for different separator thicknesses. As expected, the cell voltage decreases when the separator thickness is increased; however, the anode material utilization increases with separator thickness. This beneficial effect of a thicker separator may be a special case for the Zn/Air battery because material utilization depends strongly on the ratio of the amount of hydroxide ions to that of zinc. This is true because the separator serves as an electrolyte reservoir; and, consequently, the anode material utilization increases with the separator thickness. In selection of separator materials, it is therefore recommended that a relatively thick separator be used.

The viscosity of the electrolyte increases exponentially with the content of a gelling agent. A small amount of the gelling agent, for example, 0.5 weight percent (w/o), causes the viscosity to rise by three orders of magnitude. If transport parameters such as the electrolyte conductivity and diffusion coefficient of each species vary inversely with viscosity, the performance of the battery would be significantly affected by the content of the gelling agent. Simulations with the modified parameters based on the viscosity indicated that the cell voltage drops rapidly to the cut-off voltage with a small utilization of the active material ($<5\%$). Such a utilization is unrealistic compared to those observed in experiments. The measured conductivity of the 31 w/o KOH and 2 w/o ZnO electrolyte with various Carbopol (gelling agent) decreases by about 2% per 0.5% Carbopol (21). A possible explanation is that the gelling agent becomes a solid porous absorber for the electrolyte. Within the pores of this structure the ions of the electrolyte may pass relatively freely despite the apparently high viscosity of the phase. Therefore, the effect of gelling agent content on the transport parameters is treated in the same way as that used for a porous medium. That is, the electrolyte conductivity and diffusion coefficient of each ionic species are modified by multiplying by a correction factor according to the amount of gelling agent. Figure 15 shows the predicted effect of gelling content on the discharge curves. As can be seen, the effect of gelling agent is insignificant, the anode material utilization does not change, and the cell voltage decreases only slightly when the gelling agent changes from 0.2 to 2.2%. Therefore, the amount of gelling agent needed can be determined based simply on ease of electrolyte handling.

Conclusions

A mathematical model of a primary Zn/Air battery is presented and used to predict cell performance for particular cell designs and operating conditions. The model agrees well with experimental data and could be used to determine the optimum design parameters for other operating conditions of a primary Zn/Air battery.

Acknowledgments

LIST OF SYMBOLS

a_o	initial specific surface area of the zinc electrode, cm^2/cm^3
a_c	effective specific surface area of the cathode, cm^2/cm^3
a_p	initial value of solid zinc oxide, mol/cm^3
a_s	specific surface area of the zinc substrate, cm^2/cm^3
C_1	concentration of potassium zincate, mol/cm^3
$C_{1,e}$	equilibrium concentration of potassium zincate with zinc oxide in potassium hydroxide solution, mol/cm^3
$C_{1,e}^*$	equilibrium concentration of potassium zincate with solid potassium zincate in potassium hydroxide solution, mol/cm^3
$C_{1,ref}$	reference concentration of potassium zincate, mol/cm^3
C_2	concentration of potassium hydroxide, mol/cm^3
$C_{2,ref}$	reference concentration of potassium hydroxide, mol/cm^3
C_{O_2}	the concentration of dissolved oxygen at the interface between gas phase and electrolyte, mol/cm^3
$C_{O_2,ref}$	reference concentration of dissolved oxygen, mol/cm^3
C_t	total electrolyte concentration, mol/cm^3
$C_{t,ref}$	total electrolyte concentration at a reference state, mol/cm^3
D_A	diffusion coefficient of potassium zincate, cm^2/s
D_B	diffusion coefficient of potassium hydroxide, cm^2 s
F	Faraday constant, 96,487 C/mol
I	applied discharge current density, A/cm^2
I_1	limiting current density of the air electrode due to diffusion of dissolved oxygen, A/cm^2
$I_{1,ref}$	limiting current density of the air electrode due to diffusion of dissolved oxygen evaluated at reference alkaline concentration, A/cm^2
i_a	current density in the solid phase of the zinc electrode, A/cm^2
i_2	current density in the electrolyte phase, A/cm^2
$i_{a,ref}$	exchange current density for zinc oxidation evaluated at a reference state, A/cm^2
$i_{c,ref}$	exchange current density for oxygen reduction evaluated at a reference state, A/cm^2
j_a	transfer current per unit volume in the zinc electrode, A/cm^3
K	equilibrium constant for ZnO precipitation reaction, mol/cm^3
k_e	constant in the expression for the solubility of oxygen in KOH, cm^3/mol
k_o	a proportionality in the kinetic expression for ZnO precipitation, mol/cm^3
k_f	reaction rate constant for precipitation of zinc oxide, s^{-1}
k_{fl}	reaction rate constant for precipitation of zincate solid, s^{-1}
N_i	flux of species i, mol/cm^2-s
n	number of electrons involved in the anode reaction
n_c	number of electrons transferred in the oxygen reduction
p	reaction order with respect to hydroxide ion concentration for the cathodic reaction at the cathode
q	reaction order with respect to the concentration of dissolved oxygen for the cathodic reaction at the air electrode
R	universal gas constant, 8.314 J/mol-K

R_i'	reaction rate term in Eq. [4] that accounts for electrochemical and chemical reactions, mol/cm³-s
R_1	zincate ion reaction rate due to precipitation of ZnO and $K_2Zn(OH)_4(s)$, mol/cm³-s
R_2	hydroxide ion reaction rate due to precipitation of ZnO, mol/cm³-s
R_{ZnO}	ZnO precipitation rate, mol/cm³-s
R_k	$K_2Zn(OH)_4(s)$ precipitation rate, mol/cm³-s
s_i	stoichiometric coefficient of ionic species i in the anode reaction
$s_{c,i}$	stoichiometric coefficient of ionic species i in the cathode reaction
T	temperature, K
t	time, s
t_1	transference number for zincate ions
t_2	transference number for hydroxide ions
$\overline{V}_{Zn}$	partial molar volume of zinc, cm³/mol
$\overline{V}_{ZnO}$	partial molar volume of zinc oxide, cm³/mol
$\overline{V}_{A_s}$	partial molar volume of solid potassium zincate, cm³/mol
x	spatial coordinate, cm
x_s	the thickness of the porous zinc electrode, cm
x_l	the total length from the back side of the zinc electrode to the cathode, cm

Greek

α_a	anodic transfer coefficient of zinc oxidation
β_a	the transfer coefficient on the anodic term of the cathodic reaction at the air electrode
β_c	the transfer coefficient on the cathodic term of the cathodic reaction at the air electrode
ΔG^*	free energy change due to oversaturation, J/mol
δ	reaction zone thickness in the air electrode, cm
ϵ	porosity of either zinc electrode or the separator
ϵ_1	porosity of bare zinc in the zinc electrode
ϵ^o	initial porosity of zinc electrode
ϵ_c	porosity of the reaction zone in the cathode
ζ	correction coefficient for zincate oversaturation
η_a	the anode overpotential, V
η_c	the cathode overpotential, V
η_s	voltage loss across the separator, V
θ_u	anode material utilization, %
κ	electrolyte conductivity, S/cm
ν_{ij}	number of ionic species i per molecule of species j
ξ	correction coefficient for oversaturation
μ_i	electrochemical potential of species i, J/mol
σ	conductivity of zinc electrode, S/cm
τ	tortuosity effect constant
ϕ	electrical potential in electrolyte phase, V
ϕ_a	anode potential in the solid phase, V
ϕ_c	cathode potential in the solid phase, V
$\phi_{a,ref}$	equilibrium anode potential evaluated at reference concentrations, V
$\phi_{c,ref}$	equilibrium cathode potential evaluated at reference concentrations, V

Subscripts and Superscripts

A	$K_2Zn(OH)_4$
a	anode
B	KOH
c	cathode
o	initial or water
ref	reference state
s	separator
1	zincate ion
2	hydroxide ion

REFERENCES

1. K. W. Choi, D. N. Bennion, and J. Newman, *This Journal*, **123**, 1616 (1976).
2. K. W. Choi, D. N. Bennion, and J. Newman, *ibid.*, **123**, 1628 (1976).
3. W. G. Sunu and D. N. Bennion, *ibid.*, **127**, 2007 (1980).
4. W. G. Sunu and D. N. Bennion, *ibid.*, **127**, 2017 (1980).
5. M. J. Isaacson, F. R. McLarnon, and E. J. Cairns, *ibid.*, **137**, 2014 (1990).
6. K. G. Miller, F. R. McLarnon, and E. J. Cairns, Abstract 6, p. 8, The Electrochemical Society Extended Abstracts, Chicago, Illinois, Oct. 9-14, 1988.
7. M. Farnsworth, C. H. Kline, and J. G. Noltes, "Zinc Chemicals," Zinc Development Association, London (1973).
8. T. P. Dirkse, in "Zinc-Silver Oxide Batteries," A Fleischer and J. Lander, Editors, p. 19, Electrochemical Society, Inc., Princeton, NJ (1971).
9. T. P. Dirkse, *This Journal*, **134**, 11 (1987).
10. J. McBreen and E. J. Cairns, in "Advances in Electrochemistry and Electrochemical Engineering," H. Gerischer and C. W. Tobias, Editor, p. 273, John Wiley & Sons, New York (1978).
11. R. D. Armstrong and M. F. Bell, in "Electrochemistry," A Specialist Periodical Report, p. 1, The Chemical Society Burlington House, London (1974).
12. F. R. McLarnon and E. J. Cairns, *This Journal*, **138**, 645 (1991).
13. J. O'M Bockris, Z. Nagy, and A. Damjanovic, *ibid.*, **119**, 285 (1972).
14. J. Hendrik, A. Van Der Putten, W. Visscher, and E. Barendrecht, *Electrochim. Acta*, **29**, 81 (1984).
15. J. P. G. Farr and N. A. Hampson, *J. Electroanal. Chem.*, **13**, 433 (1967).
16. Y-C. Chang and G. Prentice, *This Journal*, **131**, 1465 (1984).
17. J. Newman and W. Tiedemann, *AIChE J.*, **21**, 25 (1975).
18. J. S. Newman and C. W. Tobias, *This Journal*, **109**, 1183 (1962).
19. "Handbook of Aqueous Electrolyte Thermodynamics: Theory & Applications," J. F. Zemaitis, D. M. Clark, M. Rafal, and N. C. Scrivener, Editors, p. 207, AIChE, New York (1986).
20. A. E. Nielsen, "Kinetics of Precipitation," Macmillan Company, New York (1964).
21. R. E. White and Z. Mao, "Mathematical Modeling of a Primary Zn/Air Battery," Final Report to NASA through MATSI, Inc. under contract, No. NAS 9-18417, June, 1991.
22. H. L. Clever "IUPAC Solubility Data Series", Vol. 7, p. 72, R. Battino, Editor, Pergamon Press, New York (1981).
23. J. S. Newman, "Electrochemical Systems," Prentice-Hall, Inc., Englewood Cliffs, NJ (1973).
24. R. Putt, MASTI, Inc. Reports to NASA, under contract, No. NAS 9-18417, 1991.
25. E. L. Littauer and J. F. Cooper in "Handbook of Batteries and Fuel Cells," p. 30, D. Linden, Editor, McGraw-Hill Book Co., New York (1984).
26. S. F. Bender and J. W. Cretzmeyer, *ibid.*, p. 10.
27. M. J. Isaacson, F. R. McLarnon, and E. J. Cairns, *This Journal*, **137**, 2361 (1990).
28. K. W. Choi and N. P. Yao in "Battery Design and Optimization," S. Gross, Editor, PV 79-1, p. 75, Electrochemical Society Softbound Proceedings Series, Princeton, NJ (1979).